ACS APPLIED MATERIALS & INTERFACES

Research Article

Cite This: ACS Appl. Mater. Interfaces 2019, 11, 38429−38439

www.acsami.org

Injectable Citrate-Based Hydrogel as an Angiogenic Biomaterial Improves Cardiac Repair after Myocardial Infarction

Zhize Yuan,[†,∥] Yung-Hao Tsou,[‡,∥] Xue-Qing Zhang,[§,∥] Shixing Huang,[†] Yang Yang,[†] Mingzhu Gao,[§] William Ho,[‡] Qiang Zhao,[*,†] Xiaofeng Ye,[*,†] and Xiaoyang Xu[*,‡,⊥]

[†]Department of Cardiovascular Surgery, Ruijin Hospital, Shanghai Jiaotong University School of Medicine, Shanghai 200025, China

[‡]Department of Chemical and Materials Engineering and [⊥]Department of Biomedical Engineering, New Jersey Institute of Technology, 323 Dr. Martin Luther King Jr. Boulevard, Newark, New Jersey 07102, United States

[§]Engineering Research Center of Cell & Therapeutic Antibody, Ministry of Education, and School of Pharmacy, Shanghai Jiao Tong University, 800 Dongchuan Road, Shanghai 200240, China

Supporting Information

ABSTRACT: Implanted medical biomaterials are closely in contact with host biological systems via biomaterial−cell/tissue interactions, and these interactions play pivotal roles in regulating cell functions and tissue regeneration. However, many biomaterials degrade over time, and these degradation products also have been shown to interact with host cells/tissue. Therefore, it may prove useful to specifically design implanted biomaterials with degradation products which greatly improve the performance of the implant. Herein, we report an injectable, citrate-containing polyester hydrogel which can release citrate as a cell regulator via hydrogel degradation and simultaneously show sustained release of an encapsulated growth factor Mydgf. By coupling the therapeutic effect of the hydrogel degradation product (citrate) with encapsulated Mydgf, we observed improved postmyocardial infarction (MI) heart repair in a rat MI model. Intramyocardial injection of our Mydgf-loaded citrate-containing hydrogel was shown to significantly reduce scar formation and infarct size, increase wall thickness and neovascularization, and improve heart function. This bioactive injectable hydrogel-mediated combinatorial approach offers myriad advantages including potential adjustment of delivery rate and duration, improved therapeutic effect, and minimally invasive administration. Our rational design combining beneficial degradation product and controlled release of therapeutics provides inspiration toward the next generation of biomaterials aiming to revolutionize regenerative medicine.

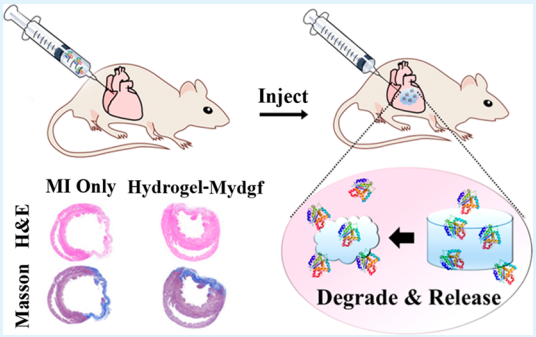

KEYWORDS: *myocardial infarction (MI), injectable hydrogel, protein delivery, cardiac remodeling, Mydgf*

1. INTRODUCTION

Hydrogels, when injected into the body, exist in close proximity with biological systems and thus need to interface with a complex, dynamically changing environment.[1,2] Cells surrounding the implant are able to sense the materials' mechanical stiffness, surface topography, and chemistry and translate these cues into signaling events which govern cell fate.[3−6] Therefore, understanding how the physiochemical properties of hydrogel implants regulate cell functions will allow researchers to mediate the cellular response. Once mastered, this groundbreaking development will herald the next generation of medical biomaterials capable of directing response of not only cells but entire biological systems. Biomaterial degradation products provide numerous signals that have been shown to modulate cellular response.[4,7,8] Specifically, it has recently been reported that degradation byproducts of citrate-presenting scaffolds lead to elevated cell energy levels which can fuel cell processes that have high metabolic demand.[3,9−11] Citrate is a key metabolic intermediate in the energy-generating processes of the mitochondria, including the TCA/Krebs cycle,[9−14] and therefore, including it in biomaterial design will provide controllable metabolic modulation in the surrounding tissue, which we hypothesize to be especially important in energy-demanding tissues in the healing heart post MI.

Ischemic heart diseases such as MI are among the major causes of death in the world.[15] MI, or heart attack, causes cardiomyocyte death, detrimental myocardial remodeling, and scar tissue formation, which results in severe cardiac dysfunction.[16] The current viable treatment options for MI are few and present numerous serious problems, such as invasive surgery, low availability of fresh hearts, thrombosis/stenosis, and immune rejection. Therefore, there is a tremendous need for novel tissue engineering solutions to address these issues. The major issues during cardiac healing include the body's inability to regenerate cardiomyocytes,

Received: July 12, 2019
Accepted: October 1, 2019
Published: October 1, 2019

DOI: 10.1021/acsami.9b12043
ACS Appl. Mater. Interfaces 2019, 11, 38429−38439

instead forming scar tissue, and the limited viability of cardiomyocytes after MI. The intramyocardial injection of therapeutics-loaded hydrogels therefore provides a novel, noninvasive method for treating ischemic MI provided there are potent therapeutics amenable for injection.

Recently, myeloid-derived growth factor (Mydgf), a newly identified paracrine-acting protein, has shown therapeutic efficacy by promoting cardiac recovery in a mouse model of MI; it increases cardiomyocyte survival and angiogenesis, attenuates scar formation, and improves cardiac dilation and systolic function.[17,18] These findings have generated widespread interest in engineering Mydgf as a potential therapeutic protein to protect and repair the heart after MI. However, days of continuous perfusion are required to maintain the therapeutic protein level, which may lead to cardiomyocyte death and injury to myocardial tissue due to prolonged administration. Moreover, in spite of the encouraging preclinical results, there remain formulation challenges due to the fragile 3D structure and low bioavailability of Mydgf. Therefore, injection of a Mydgf-loaded hydrogel is a potential method to both maintain the local therapeutic dose in the infarcted myocardium over extended periods following a single injection and increase bioavailability.

Here, we report a robust citrate-presenting injectable hydrogel preparation method and an approach for local sustained delivery of Mydgf for post-MI heart regeneration. The hydrogel can be synthesized with biocompatible starting chemicals including citric acid and poly(ethylene glycol)-diol. Importantly, a green chemistry enzymatic functionalization approach has been utilized for hydrogel fabrication. The injectable citrate-based polymeric hydrogel (1) is minimally invasive, (2) serves as a biodegradable scaffold to provide structural support for the injured myocardium, (3) releases the encapsulated Mydgf for a prolonged period of time, (4) promotes angiogenesis and cardioprotecton via the citrate degradation byproducts by activating the PI3K-Akt-mTOR pathway and manipulating the citric acid cycle,[3,9,11] (5) provides a tunable release profile of encapsulated protein therapeutics, and (6) shows significant improvement in therapeutic effect by local delivery of Mydgf. Finally, our bioactive hydrogel scaffold can be easily tuned for practically any biological application of interest, thus offering immense potential for future clinical therapies.

2. RESULTS AND DISCUSSION

2.1. Polymer Synthesis, Characterization, and Hydrogel Fabrication. To synthesize the citrate-based polyester hydrogel, citrate acid and polyethylene glycol reaction proceeded via a facile polycondensation reaction. The yielded polyester oligomers poly(polyethylene glycol-*co*-citrate) (PPC) were then reacted with an ethyl ester of a thiol acid; this reaction was catalyzed by CALB-immobilized acrylic resin. The aforementioned transesterification reaction introduces multivalent thiol functional groups (Scheme 1).

The ^{1}H NMR (Bruker 500 MHz) spectra (500 MHz, DMSO-d_6, δ) of PPC (Figure S1a) and PPC-ET (Figure S1b) showed the presence of the peaks at 2.6−2.9 ppm (−CH_2− from citric acid), 3.3−3.6 and 4.05−4.2 ppm (−OCH_2CH_2− from hexaethylene glycol), and 3.2 and 1.9 ppm from −CH_2− of −CH_2SH and −SH, respectively, which determined the chemical structures of the polyester oligomers. PPC-ET molecular weight (~2023 Da) was measured by MALDI-TOF-MS (Bruker). Ellman's reagent showed there were 4−5 thiol groups conjugated on each PPC-ET oligomer.

Scheme 1. Synthesis Schematic of Polyester Oligomers 1 (PPC) and 2 (PPC-ET).

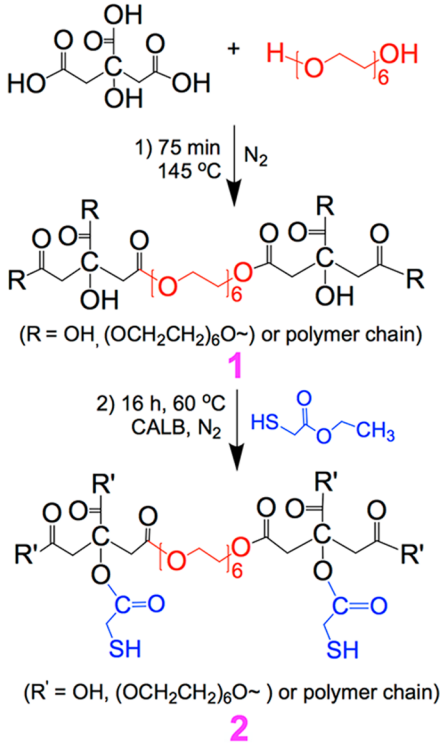

Hydrogels were fabricated by using thiol-Michael addition chemistry (Figure S2) according to a similar procedure described in detail previously.[19] Briefly, 8-arm PEG-maleimide and PPC-ET were dissolved in phosphate-buffered saline (PBS) separately to acquire precursor solutions with predetermined weight concentrations. PPC-ET/PEG hydrogels could be fabricated in situ by mixing the two precursor solutions. More details can be found in the Experimental Section.

2.2. Degradation, Gelation, and Mechanical Properties of PPC-ET/PEG Hydrogels. The mechanical characteristics and sol-to-gel transition of hydrogel disk samples fabricated by combining PPC-ET oligomer and 8-arm PEG-maleimide in different buffers (1X PBS and 5X PBS, pH = 7.4) at different initial cured polymer mass percentages (5 and 10 wt %) were characterized using dynamic rheology. The time points where storage and loss modulus crossed over (i.e., tan (δ) = G'/G'' = 1) were used to define the onset of gelation. The results demonstrated that a rise in polymer fraction from 5 to 10 wt % resulted in a greater than 12-fold increase in G' along with a significant decrease in gelation time (Figure 1a−c). This is hypothesized to be caused by the presence of more cross-linked networks when increasing the content of PEG and PPC-ET oligomer, which leads to increased storage modulus. Hydrogels formed in the 5X PBS also exhibited a stronger storage modulus (Figure 1a and 1b) and quicker sol-to-gel transition (Figure 1c), representing the increased reactivity of thiol-maleimide conjugate addition at higher ionic strength. Additionally, the PPC-ET/PEG hydrogels cured with higher initial polymer mass (10 wt %) exhibited lower equilibrium swelling ratios (Q_m) (Figure 1d). The low-to-moderate swelling behavior and network characteristics of 10 wt %

DOI: 10.1021/acsami.9b12043
ACS Appl. Mater. Interfaces 2019, 11, 38429−38439

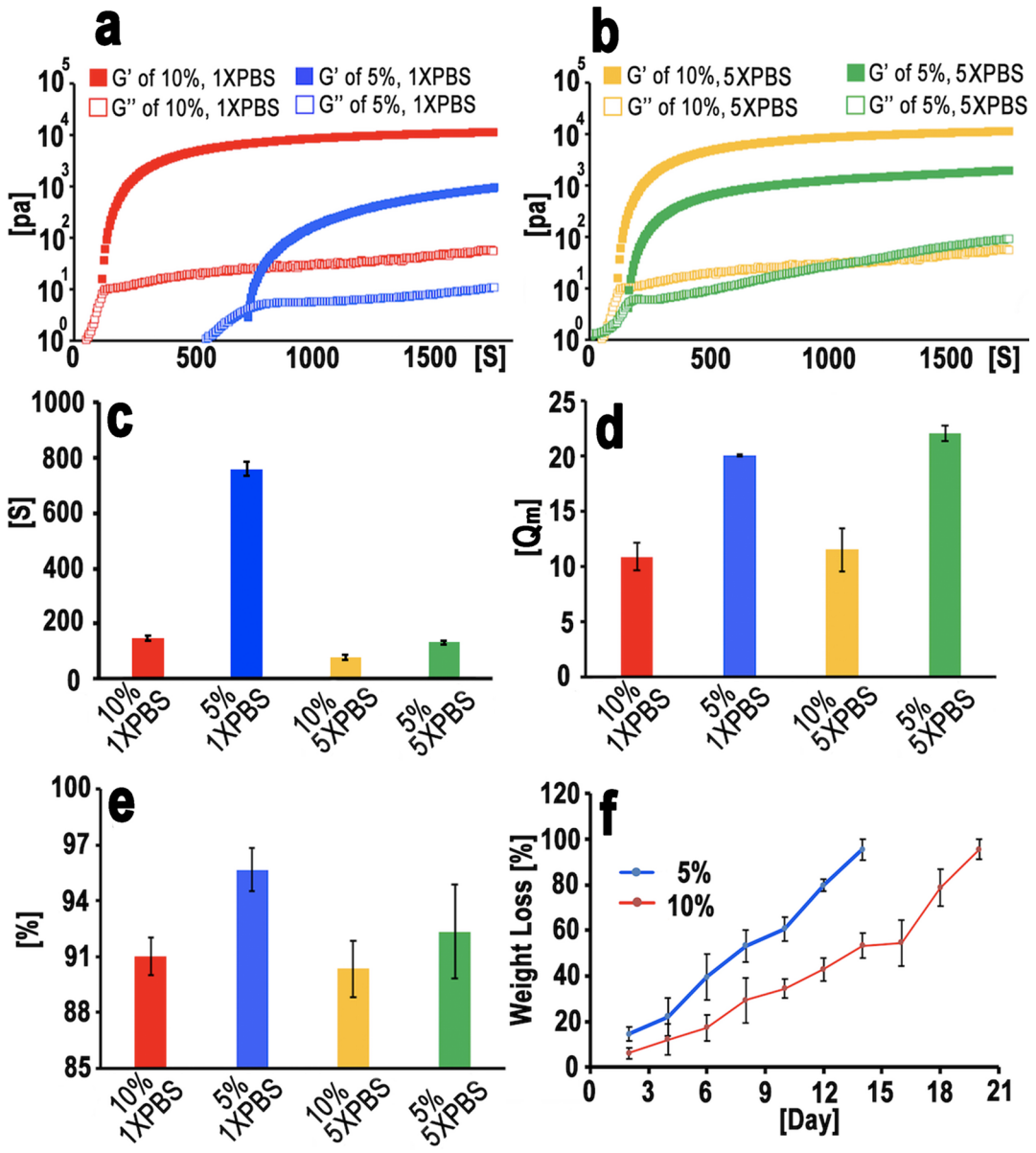

Figure 1. Characterization of PPC-ET/PEG-based hydrogels. (a and b) Dynamic rheology curves for the PPC-ET/PEG hydrogels with different polymer concentrations and solvents, where G' is defined as the storage modulus (filled symbols) and G'' defined as loss modulus (empty symbols). (c) Gelation time, (d) water uptake, and (e) porosity of PPC-ET/PEG-based hydrogels with different formulations. (f) Degradation profile of PPC-ET/PEG-based hydrogel with 5 and 10 wt % polymer concentrations.

hydrogels offer potential benefits for their effective use in enclosed (fixed volume) in vivo environments.

The injectable hydrogels provide spatiotemporal control of the release of therapeutics through drug diffusion and material degradation. Porosity and microstructure morphologies have a great impact on the rates of drug diffusion through the hydrogel mesh or the water-filled pores. As shown in Figure 2a and 2b, a loose, porous, and interconnected appearance was observed for the PPC-ET/PEG hydrogels cured with 5 wt % polymer mass. Compared with 5 wt % hydrogels, 10 wt % hydrogels had a tighter and denser structure, suggesting a relatively higher cross-link density (Figure 2c and 2d). This was consistent with their porosity characterization (Figure 1e). Figure 1f shows that increasing the initial polymer mass percentage prolonged hydrogel degradation, confirming the influence of cross-link density on material degradation. Ten weight percent PPC-ET/PEG hydrogels demonstrated a more extended degradation timeline of up to 21 days compared to 5 wt % hydrogels. These results indicate that mechanical attributes, degradation rate, and gelation kinetics of the PPC-ET/PEG hydrogels can be tailored by adjusting polymer mass percentage, cross-linking conditions, and solvent buffer conditions.

To demonstrate the utility of the PPC-ET/PEG hydrogels for protein delivery, the release profiles of therapeutic protein from hydrogels were measured using BSA as a model protein. BSA was encapsulated within 5 or 10 wt % hydrogels, and in vitro release studies were performed in PBS (pH 7.4) at 37 °C. The cumulative protein release profiles from both 5 and 10 wt % hydrogels showed a preliminary (~25% of the initial loading) burst release in the first 6 h, followed by a sustained, slower release period of up to 144 h (Figure 2e). Protein

DOI: 10.1021/acsami.9b12043
ACS Appl. Mater. Interfaces 2019, 11, 38429−38439

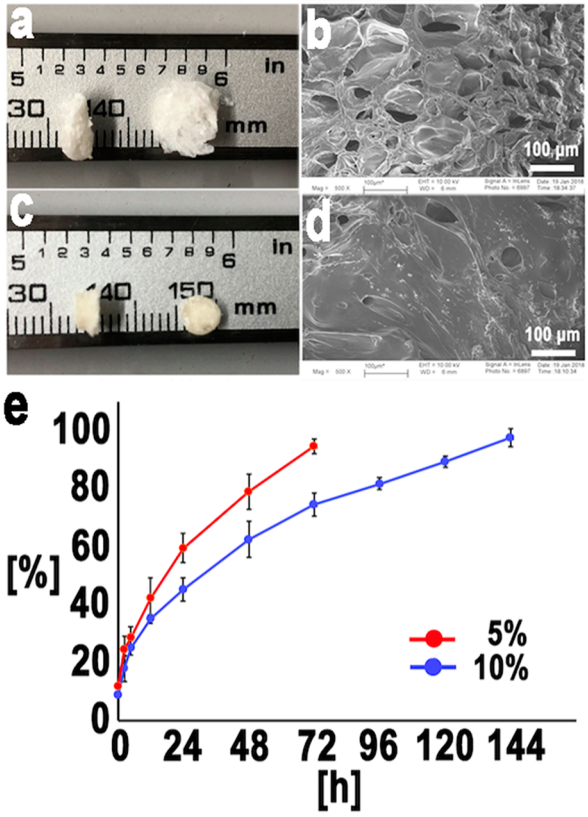

Figure 2. Images of 5 (a) and 10 (c) wt % PPC-ET/8-arm PEG-maleimide hydrogels after lyophilization. SEM images of PPC-ET/8-arm PEG-maleimide samples in different concentrations: (b) 5 and d) 10 wt %. (e) In vitro release of bovine serum albumin from 5 and 10 wt % hydrogels. Data is presented as the mean ± standard deviation (n = 5).

diffusion was delayed about 72 h when released from the dense 10 wt % hydrogel due to the lower swelling ratio, dense structure, and delayed degradation rate, resulting in a slower protein release compared to the porous 5 wt % hydrogel. The results showed that the PPC-ET/PEG hydrogels were capable of loading therapeutic protein and allowed for sustained release. The mechanisms of release are likely influenced by diffusion, the material's structure, and polymer degradation.

2.3. In Vitro Biocompatibility Evaluation. XTT assay was utilized to evaluate the cytotoxicity of PPC-ET/PEG hydrogels formed through cross-linking of PPC-ET oligomer and 8-arm PEG-maleimide in various buffers (1X PBS and 5X PBS, pH = 7.4) at initial cured polymer mass percentages of 5 and 10 wt %. Cell viabilities following 2 days culture of NIH-3T3 with extracts from each of the four different hydrogels are shown in Figure 3a. The cell viabilities measured were comparable to the control group (cell culture plate), demonstrating that the degradation byproducts of the PPC-ET/PEG hydrogels are well tolerated and minimally cytotoxic. Since the building blocks of the PPC-ET/PEG hydrogels are a nontoxic metabolic product (citric acid) and PEG (which is FDA-approved), the resultant hydrogel would logically be biocompatible as well. Furthermore, Michael addition cross-linking can be performed under mild conditions and does not involve cytotoxic moieties.[20] Maleimide groups of 8-arm PEG were partially modified with extracellular matrix (ECM)-derived peptide CRGDS (to encourage cell adhesion and proliferation) and then reacted with PPC-ET in 1X PBS to yield 10 wt % CRGDS-functionalized PPC-ET/PEG hydrogel (Figure 3b). NIH-3T3 cells were cultured onto the peptide-functionalized hydrogel, and cell proliferation data were recorded to characterize hydrogel biocompatibility. As shown in Figure 3c, the CRGDS-functionalized PPC-ET/PEG hydrogel facilitated cell adhesion and spreading, with the hydrogel surface completely covered by cells by 48 h. Our findings highlight the excellent in vitro biocompatibility and design flexibility of the injectable hydrogel implant, making it a versatile platform for local noninvasive in vivo drug delivery.

2.4. Mydgf-Loaded Hydrogel Promotes Tubular Formation in HUVECs. The endothelial tube formation assay provides a tool for the assessment of angiogenesis in vitro. In the present study, endothelial cells were cultured in a gel of membrane extract and the ability to form tube-like structures was assessed. Endothelial cells obtained from the human umbilical vein (HUVECs) were used for this in vitro tube-formation assay. The growth factor-reduced basement membrane extract Matrigel matrix was used as a culture substratum. Briefly, a thin layer of PPC-ET/PEG hydrogels (300 μL) and Mydgf-loaded hydrogels (50 ng/mL) was laid over the prechilled 96-well culture plates, while the control group was coated with growth factor-reduced Matrigel matrix until completely solidified. HUVECs were cultured in Dulbecco's Modified Eagle Medium/F12 supplemented with endothelial cell growth supplement (ECGS) at 37 °C and 5% CO_2. Trypsinized HUVECs resuspended in DMEM medium with only PBS and Mydgf (50 ng/mL) were added to the preconditioned culture plates at a density of 2×10^4 cells/well, respectively.

After 8 h incubation, tubular numbers of each treatment group were observed and counted under a light microscope (200×) (Figure 3d). The free Mydgf and Mydgf−hydrogel treatment groups significantly promoted tubular formation of HUVECs compared to the PBS and hydrogel control groups in terms of tubular number (Figure 3e) and tubular intersecting nodes (Figure 3f). It has been shown that Mydgf acts on endothelial cells through increased phosphorylation of mitogen-activated protein kinases (MAPK) 1 and MAPK3 as well as STAT3 on S727 and stimulates the transcriptional activity of STAT3, leading to increased proliferation.[17] It is noteworthy that the Mydgf released from the hydrogel is as effective as the free protein in promoting angiogenesis and tubular formation in HUVECs, showcasing the ability of the 10 wt % PPC-ET/PEG hydrogel to maintain therapeutic protein activity and release active protein. Additionally, citrate-presenting hydrogel alone (without Mydgf) can also promote tubular formation (Figure 3e), which is consistent with our previously observed angiogenic effect of citrate for upregulating the expression of CD31 (Figure S3a) and VEGF (Figure S3b) in HUVECs via activation of the P13K-Akt-mTOR pathway.

2.5. Rat AMI Model and Evaluation of Heart Functions after Hydrogel Injection. To better understand how the citrate-based hydrogel can improve cardiac repair after MI, 10 wt % PPC-ET/PEG hydrogels (1XPBS) loaded with Mydgf were used. Rats were anesthetized with pentobarbital sodium (30 mg/kg, i.p.), orally tracheal intubated, and ventilated. After a left thoracotomy was finished in the fourth intercostal ribs, the left anterior descending artery (LAD) of the heart was exposed and ligated permanently with 6−0 polypropylene for induction of acute myocardial infarction (AMI). Successful AMI was confirmed by left ventricle (LV)

DOI: 10.1021/acsami.9b12043
ACS Appl. Mater. Interfaces 2019, 11, 38429−38439

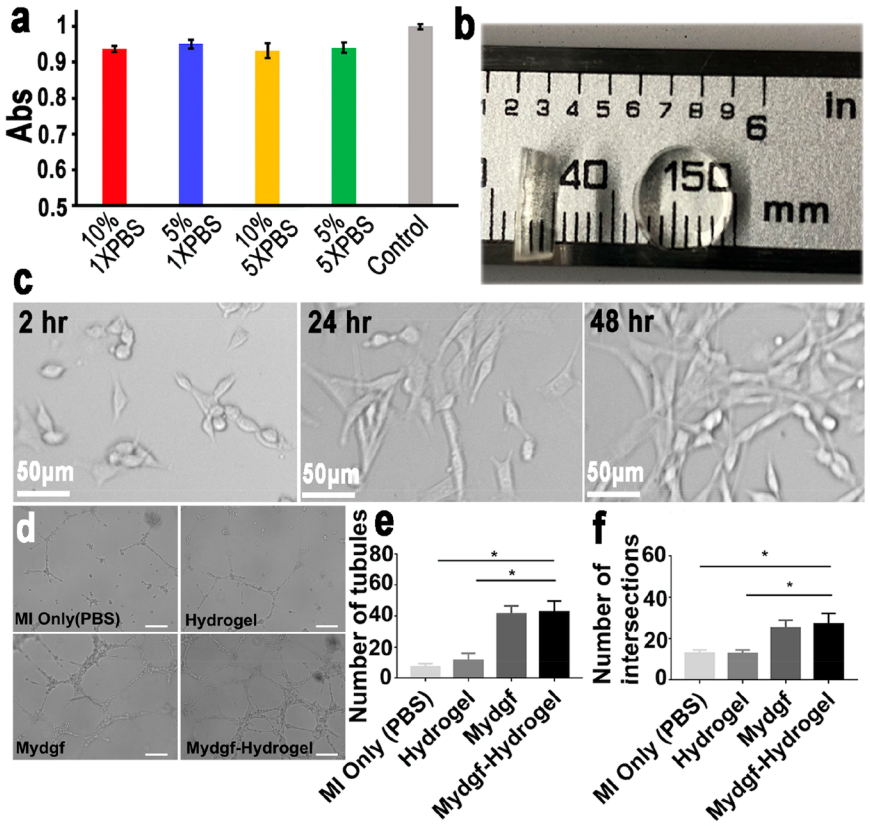

Figure 3. In vitro cytocompatibility studies of the hydrogel. (a) Cytotoxicity test of PPC-ET/PEG-based hydrogels with a control after being incubated for 48 h. (b) Image of disk-like PPC-ET/PEG-based hydrogels. (c) NIH-3T3 cell attachment and proliferation on the PPC-ET/PEG-based hydrogels (10×). Effect of Mydgf on tubular formation in vitro (200×). Scale bar 100 μm. (d) Richly formed tubular structure was observed in the Mydgf and Mydgf−hydrogel groups compared with the PBS and hydrogel groups. Bar charts show numbers of (e) tubules and (f) intersecting nodes between different groups. Data were represented as mean ± SEM of three independent experiments; (*) $p < 0.05$.

ligation regional wall paleness and ST-segment elevation on an electrocardiogram (ECG) device. Twenty nine gauge insulin syringes with PBS (MI-only), control hydrogel (no Mydgf), Mydgf, and Mydgf−hydrogel (10 μg of Mydgf encapsulated in 120 μL of sterile well-mixed hydrogel precursor solutions) were prepared during the surgery. PPC-ET/PEG hydrogels were formed in situ within seconds before injection. After LAD ligation, the heart was to randomly receive one of the above four groups' treatments. A total volume of 120 μL of hydrogel or reagents was injected directly into 3 locations (the peri-infarct left ventricle wall and MI zone) after LAD ligation before closure of the thorax.

As a noninvasive technology, echocardiography was used to evaluate cardiac function recovery after Mydgf−hydrogel treatment. Rats received echocardiography 2 days after LAD permanent ligation (baseline) and 4 weeks post-treatment to measure cardiac function. Heart structure indicators such as systolic left ventricular internal dimension (LVIDs), diastolic left ventricular internal dimension (LVIDd), left ventricular ejection fraction (LVEF), and left ventricular fractional shortening (LVFS) measurements indicated a comparable baseline cardiac injury between all groups (Figure S4). These high-quality images were determined from short-axis 2-dimensional imaging at the midpapillary level. Representative M-mode images at 4 weeks after treatment showed that relative left ventricular segmental regional wall-motion abnormalities, weak myocardial contraction, left ventricular cavity enlargement, and wall myocardium thickness decreased in all MI rats (Figure 4a). From short-axis imaging, heart structure parameters such as LVIDs, LVIDd, and LVEF and fractional shortening were also calculated.

LVEF is a parameter of the percentage of blood ejecting the heart each time it contracts, and a decrease was defined by the American Heart Association as a measurement of heart failure. The Mydgf−hydrogel group showed distinctly increased LVEF (51.3 ± 1.0%) in comparison to PBS, hydrogel, and Mydgf groups (37.1 ± 0.7%, 39.5 ± 0.6%, and 43.7 ± 0.7%, respectively, Figure 4b). For further evaluation of the heart function, the LVFS was calculated as follows: (LVIDd-LVIDs)/LVIDd. Likewise, injection of Mydgf−hydrogel made a marked increase on the LVFS (27.0 ± 0.9%) in comparison to the PBS, hydrogel, and Mydgf groups (18.7 ± 0.4%, 20.2 ± 0.3%, and 22.6 ± 0.5%, respectively, Figure 4c). Moreover, the Mydgf−hydrogel group showed the least increase in LVIDs (5.38 ± 0.17 mm) in comparison to PBS, hydrogel, and Mydgf treated groups (7.38 ± 0.28, 6.74 ± 0.5, and 6.15 ± 0.31 mm, respectively, Figure 4d). A parallel tendency was also observed for the LVIDd, where the Mydgf−hydrogel group showed the lowest increase in LVIDd (7.38 ± 0.28 mm) in comparison to PBS, hydrogel, and Mydgf groups (9.10 ± 0.34, 8.45 ± 0.35, and 7.94 ± 0.43 mm, respectively, Figure 4e). From the above cardiac echocardiography results, heart structure parameters from the 4 groups indicated a substantial benefit from Mydgf−hydrogel regarding heart functions such as LVEF and LVFS. In order to study regenerated infarcted myocardial tissues after MI, small-animal

DOI: 10.1021/acsami.9b12043
ACS Appl. Mater. Interfaces 2019, 11, 38429−38439

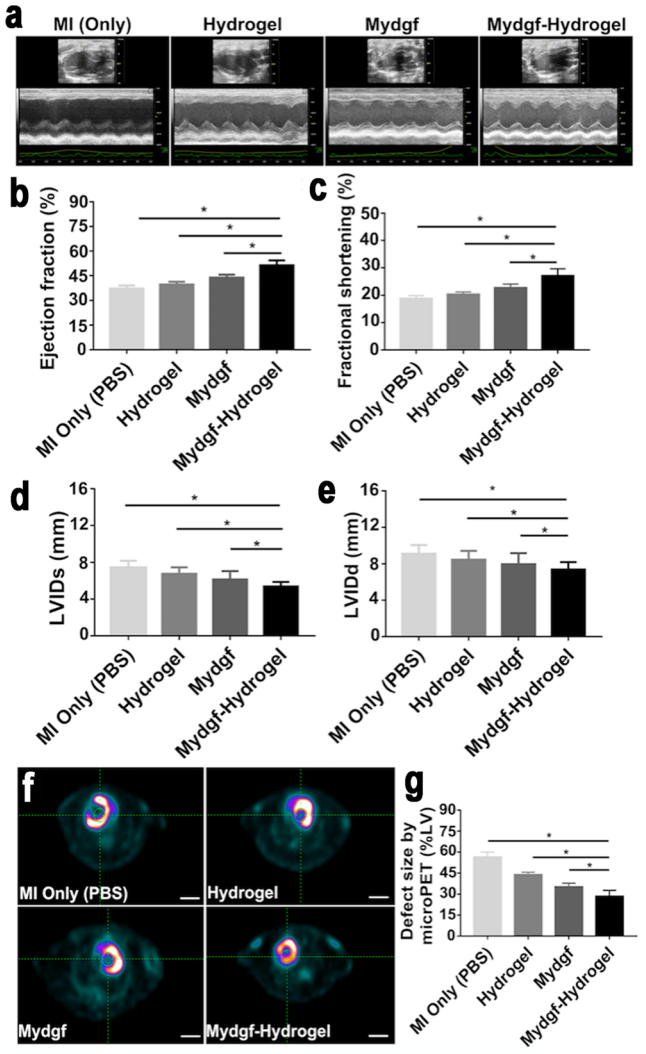

Figure 4. Evaluation of myocardial function and viability. (a) Representative echocardiographic images for 4 weeks after treatment. (b) LVEF, (c) FS, (d) LVIDs, and (e) LVIDd were assessed with two-dimensional echocardiography. (f) Short-axis images of myocardial ^{18}F-fluorodeoxyglucose (FDG) uptake acquired with a small-animal PET system. Scale bar: 10 mm. (g) Percentage of LV ^{18}F-FDG uptake defect size was measured. Data were represented as mean ± SEM; (*) $p < 0.05$.

positron emission tomography (PET) was used for the assessment of the treatment efficacy in this study. PET has been applied widely in the field of cardiology for the use in the assessment of myocardial ischemia and viability. PET presents excellent spatial resolution and enables quantitative measurements of the ^{18}F-fluorodeoxyglucose (FDG) tracer uptake (viable myocardium shows high ^{18}F-FDG uptake). The tracer is used as an indicator of the viable myocardium tissue, and uptake of ^{18}F-FDG has also been applied to assess the MI size. ^{18}F-FDG PET can be used to locate areas of myocardial viability (^{18}F-FDG uptake area) and necrosis (^{18}F-FDG uptake defect area) and to collect information on the effectiveness of the post-MI treatments. In the present study, short-axis images of myocardial ^{18}F-FDG uptake in the LV of 4 groups of rats were acquired with a small-animal PET system. LV myocardium showed excellent contrast of ^{18}F-FDG. The percentage of LV ^{18}F-FDG uptake defect size was measured (Figure 4f). The Mydgf–hydrogel group showed a marked decrease in the defect size (28.4 ± 1.5%) in comparison to the PBS, hydrogel, and Mydgf groups (56.4 ± 1.3%, 43.7 ± 0.7%, and 35.1 ± 1.0%, respectively, Figure 4g).

Compared with echocardiography, PET has an additional advantage: it can be used in the assessment of defect size, myocardial viability, and metabolism. Additionally, PET is also effective in monitoring cardiac physiology at the metabolic level. In this study, the PET results demonstrated that the Mydgf–hydrogel treatment markedly decreased the defect size compared to the PBS, hydrogel, and Mydgf groups. From the above cardiac echocardiography and PET results, it can be seen that a significant improvement of heart function and increased myocardial viability was achieved after Mydgf–hydrogel administration. As imaged with a micro-PET, ^{18}F-FDG uptake in the MI rat model correlates well with MI size measured by histological studies.

2.6. Morphometric and Histological Studies for Heart Structure Evaluation. In order to understand cardiac remodeling changes at the tissue level and evaluate therapeutic efficacy of the hydrogel combined with Mydgf in vivo, we investigated left ventricular wall structure and fibrosis 4 weeks post injection. Hematoxylin and eosin (H&E) staining and Masson's trichrome staining were performed on heart samples as a histological analysis (Figure 5a). As shown in H&E staining, the LV wall was observed to be much thicker in the animals of the Mydgf–hydrogel-treated group as compared to the other three groups.

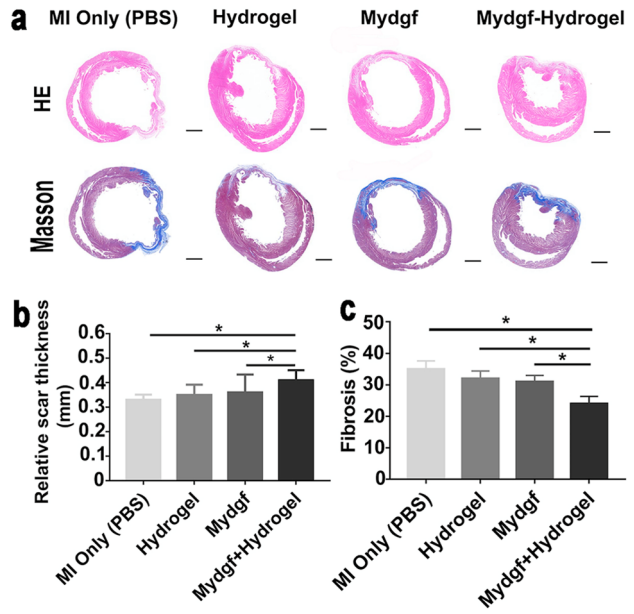

Figure 5. Morphologies and histology of the LV. (a) H&E and Masson's trichrome staining. Scale bars, 2 mm. (b) Quantification analysis of the relative scar thickness. (c) Percent fibrosis of the severity of interstitial fibrosis. Data were represented as mean ± SEM; (*) $p < 0.05$.

Interstitial fibrosis may become dysregulated in the infarct region and extend to noninfarct zones because of the massive collagen deposition after MI, which contributes to LV remodeling and dysfunction. A large area of collagen deposition can be seen (blue) in the MI border zone, indicating an infarcted myocardium and scar formation. The MI hearts treated by injectable Mydgf–hydrogels were significantly less fibrotic. An adverse cardiomegaly was

DOI: 10.1021/acsami.9b12043
ACS Appl. Mater. Interfaces 2019, 11, 38429–38439

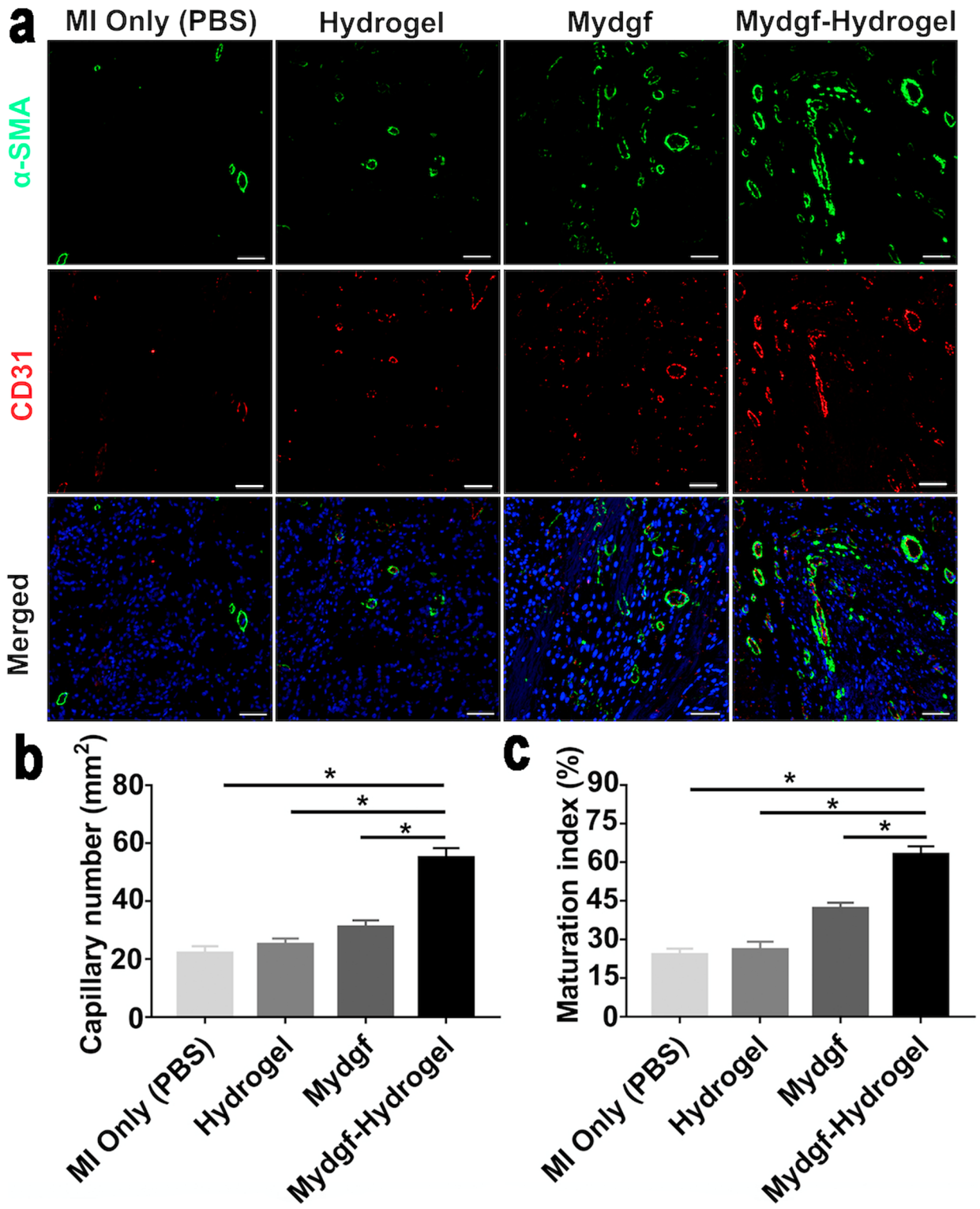

Figure 6. Immunofluorescence assessment of the vascularization 4 weeks after treatment. (a) CD31 (red) and α-SMA (green) staining for the blood vessels. Scale bar: 50 μm. Quantification of the (b) capillary density and (c) maturation index. Increased capillary density and maturation index are shown in the group treated with the Mydgf–hydrogel relative to the changes in the other groups. Data are expressed as the mean ± SEM; (*) $p < 0.05$.

observed in PBS and hydrogel groups but to a much lesser degree in Mydgf groups and Mydgf–hydrogel group. The relative scar thickness in the Mydgf–hydrogel treatment group showed a sharp increase (0.41 ± 0.04 mm) over the PBS, hydrogel, and Mydgf treated groups (0.33 ± 0.02, 0.35 ± 0.04, and 0.36 ± 0.07 mm, respectively, Figure 5b). Compared with the PBS (42 ± 2.64%), hydrogel (36 ± 2.45%), and Mydgf groups (34 ± 2.23%), the Mydgf–hydrogel-treated group (25 ± 2.36%) showed a significant reduction in infarct size (Figure 5c). The cardiac remodeling seen after MI often causes adverse effects such as cardiomyocyte loss, heart dysfunction, and eventually heart failure.[21] Masson's trichrome staining results

DOI: 10.1021/acsami.9b12043
ACS Appl. Mater. Interfaces 2019, 11, 38429–38439

showed a dramatic elevation in relative scar thickness and a significant reduction in the severity of interstitial fibrosis in the Mydgf−hydrogel treatment group, demonstrating more favorable results compared to the other three treatment groups. This result is consistent with differences in LVIDd, LVIDs, and LVFS values measured in echocardiography, as well as the Micro-PET uptake results. This factor may be responsible for the cardioprotective effect of Mydgf. It reveals that Mydgf−hydrogel treatment groups trend toward decreased infarction size, fibrosis levels, and increased LV wall thickness.

2.7. Immunohistochemistry in the Evaluation of Neovascularization. Regarding the aspects of cardiac regeneration and functional recovery, revascularization of ischemic myocardium is of great importance.[22] Increasing myocardial capillary density is an effective strategy to restore blood and nutrient supply in ischemic MI tissue through angiogenesis. Double staining of the heart tissue sections for α-SMA (vascular smooth muscle cell marker) and CD31 (endothelial cell marker) was performed to analyze microvasculature formation, which could be visualized by fluorescence microscopy. To study the angiogenesis process, we costained CD31 and α-SMA antibodies in heart tissue at 4 weeks after injection treatments (Figure 6a). We observed a higher number of neovessels in the Mydgf−hydrogel treatment group (55 ± 3.31 mm^{-2}) compared to PBS, hydrogel, and Mydgf groups (22 ± 2.43, 25 ± 2.12, and 31 ± 2.36 mm^{-2}, Figure 6b). The Mydgf−hydrogel treatment (63 ± 3.21 mm^{-2}) resulted in a significantly higher presence of mature neovessels than PBS, hydrogel, and Mydgf treatments (24 ± 2.43, 26 ± 3.12, and 42 ± 2.26 mm^{-2}, respectively) (Figure 6c). The results illustrate the capability of the Mydgf-hydrogel treatment in promoting the generation of robust angiogenesis with mature neovasculature. This is an expected result considering the previously reported angiogenic capabilities of Mydgf; the induction of mature vessels would be expected to improve blood flow, contributing to less ischemia in the MI region. Under the influence of the controlled release of this growth factor, enhanced angiogenesis in the Mydgf−hydrogel group is made possible. The local and sustained intramyocardial delivery of Mydgf attenuated the adverse LV remodeling and induced angiogenesis after MI. In addition, the induction of neovascularization is an important element in evaluating the therapeutic efficacy of interventions for MI, as reducing damage to ischemic myocardium depends on the vasculature being present.[23] The Mydgf−hydrogel induces an increase in neovascularization, which aids in relieving the ischemia in the infarct area. On the basis of these findings, recovery of cardiac function may be possible via revascularization.

2.8. Terminal Deoxynucleotidyl Transferase-Mediated dUTP Nick End Labeling (TUNEL) Staining To Measure Apoptosis. Apart from angiogenesis, previous research has indicated that cell apoptosis also plays a fundamental role in MI. LV remodeling after MI is associated with myocyte apoptosis in myocardium and is related to contractile dysfunction. Using an ischemia-reperfusion (I/R) injury model in vitro, it has been shown that the recombinant Mydgf exerts cardiomyocyte-protective effects through PI3K/Akt signaling pathway, which inhibits the intrinsic apoptosis. The I/R model in Mydgf-deficient mice treated with Mydgf revealed that Mydgf is required and sufficient to prevent cardiomyocyte apoptosis and decrease myocardial infarct size.[17] As apoptosis is an inevitable outcome of MI, in the present study, TUNEL staining was used to determine apoptosis in the cardiomyocytes as a measure of their survival (Figure S5a). Compared with the PBS, hydrogel, and Mydgf groups, there were fewer TUNEL positive (apoptotic) cells within the border zone of the Mydgf−hydrogel treatment group (Figure S5b). A significant decrease in myocardial apoptosis such as that shown in this study might provide additional beneficial effects in protecting cardiac dysfunction. These results indicate that the angiogenesis in the infarct zone induced by the Mydgf−hydrogel may be the factor preventing the radially extending apoptotic process seen in the PBS and hydrogel controls, enabling survival of hypertrophied myocytes within the peri-infarct zone and improving myocardial function.

3. CONCLUSION

In summary, this work focused on developing a citrate-based polyester hydrogel capable of Mydgf delivery, and the post-MI remodeling efficacy of this Mydgf−hydrogel was evaluated. We demonstrated that this polyester hydrogel is well suited for the local, controlled, intramyocardial delivery of Mydgf. Injection of the Mydgf−hydrogel into the LV of rats with MI showed significant improvements in cardiac morphology and functionality at 4 weeks relative to the controls. We further investigated the functional roles of the Mydgf−hydrogel in promoting angiogenesis and reducing cardiac cell apoptosis. It is noteworthy that hydrogel alone without Mydgf also showed benefits in thickening the myocardium and cardiac function when injected directly after infarction partially due to the angiogenetic effects of the hydrogel degradation product citrate, indicating great potency as an injectable biomaterial for regenerative medicine. Future work will focus on the study of synergistic effects between released citrate and encapsulated therapeutics in tissue engineering.

On the basis of these results, the developed citrate-based polyester hydrogel shows excellent biocompatibility as an injectable medical material with the capability to release Mydgf for prolonged periods of time. Furthermore, our hydrogel/growth factor codelivery method showed benefits regarding cardiac function post-MI, notably reducing apoptosis and adverse cardiac remodeling, increasing angiogenesis, and improving cardiomyocyte survival. The polyester hydrogel can be also used as an implant biomaterial for applications of drug delivery and tissue engineering with clinical translational potential.

4. EXPERIMENTAL SECTION

Materials. Citric acid, poly(ethylene glycol) ($M_w \approx 200$ kDa), ethyl thioglycolate, *Candida antarctica* Lipase B (CALB), bovine serum albumin (Mw: 68 kDa), and Cell Proliferation Kits (XTT) were purchased from Sigma-Aldrich (St. Louis, MO, USA). 8-Arm PEG with terminal maleimide groups ($M_w = 10$ kDa) were purchased from JenKem Technology (Plano, TX, USA). Ellman's reagent was purchased from Thermo Fisher Scientific (Waltham, MA, USA). All chemicals were used as received without further purification. Dialysis tubes (0.5−1 kDa) were purchased from Spectrum (Houston, TX USA). Dulbecco's Modified Eagle's medium (DMEM), fetal bovine serum (FBS), and mouse fibroblast NIH-3T3 were purchased from American Type Culture Collection (ATCC) (Manassas, VA 20110 USA). Human umbilical vein endothelial cells (HUVECs) were obtained from American Type Culture Collection (ATCC, Rockville, MD, USA). Matrigel matrix was purchased from BD Biosciences (CA, USA). Recombinant Mydgf was obtained from Novoprotein (Shanghai, China).

DOI: 10.1021/acsami.9b12043
ACS Appl. Mater. Interfaces 2019, 11, 38429−38439

Synthesis of Polyester Oligomers (PPC and PPC-ET) and CRGDS-Functionalized 8-Arm PEG Derivatives. Synthesis steps were similar to previous work with little modification.[24] Briefly, poly(polyethylene glycol-*co*-citrate) polyester oligomer (PPC) was first synthesized via a facile polycondensation reaction (Figure S1). Citric acid was reacted with an equimolar amount of PEG under mild stirring at 145 °C for 75 min. After cooling to room temperature, the PPC oligomer was purified through a dialysis method followed by freeze drying.

PPC-ET was synthesized through the transesterification of PPC with ethyl thioglycolate using CALB as the catalyst.[25] The PPC was first dissolved in organic solvent (acetonitrile); ethyl thioglycolate and CALB (5:1 molar ratio of ethyl thioglycolate to citric acid) were added to the reaction after PPC was completely dissolved in acetonitrile. The reaction was stirred at 60 °C for 16 h under nitrogen protection. The reaction stopped by being filtered out of CALB, and the resultant PPC-ET oligomer was purified through a dialysis method followed by lyophilization.

8-Arm PEG-maleimide-CRGDS was used to formulate peptide-functionalized hydrogels for in vitro cell culture studies. CRGDS and 8-arm PEG-maleimide (molar ratio 1:1) were dissolved in PBS (pH = 7.4) with triethanolamine[26] for 60 min. The product was purified by a dialysis bag (3500 kDa) followed by lyophilization for 3 days.

Dynamic Rheology Measurement. Sol-to-gel kinetics and mechanical properties of hydrogels were measured by using a Discovery Hybrid Rheometer 3 (TA, Instruments, New Castle, DE). Prior to the measurement, the hydrogel precursor solutions were mixed with a volume of 280 μL and applied to a temperature control stage at 37 °C. Dynamic time sweep measurements were made within the linear viscoelastic region (strain = 5%, angular frequency = 1 rad s^{-1}). The operation time of 15 s has been added to the data.

Swelling and Porosity Measurement. Hydrogel disk samples (~120 μL, diameter = 8.1 mm; height = 3.0 mm) were cured in disk silicone molds at room temperature. The cured hydrogel samples were immersed in PBS (pH = 7.4) solution at 37 °C/5% CO_2 for 24 h to remove the unreacted fraction. The initial dry hydrogel weight (W_0) was measured after lyophilization. Next, samples were incubated in PBS (pH = 7.4) solution at 37 °C/5% CO_2 for at least 6 h to achieve equilibrium status. After the excess water was removed with a filter paper, the weight of swollen hydrogel was recorded as wt. The swelling ratio (Q_m) calculation is

$$Q_m = (W_t/W_0) \times 100\% \quad (1)$$

The porosity of the hydrogels was measured by a liquid displacement method.[27] The freeze-dried hydrogel samples were immersed in DI water (volume known, V_1) in the beaker for 1 h. The total volume (hydrogels + DI water) was recorded as V_2, and the volume of DI water remaining in the beaker was recorded as V_3 after the hydrated hydrogel samples were removed. The porosity (P) of the scaffold was calculated as

$$P\ (\%) = [(V_1 - V_3)/(V_2 - V_3)] \times 100\% \quad (2)$$

Morphology of Hydrogels. Scanning electron microscopy (SEM) was used to observe the morphology of the hydrogel samples. The hydrogel samples were freeze dried and coated with a 20 nm layer of gold using a sputter coater. Test samples were blown clean using compressed air before SEM characterization.

In Vitro Degradation of Hydrogels. For degradation studies, hydrogels (~120 μL, diameter = 8.1 mm; height = 3.0 mm) were lyophilized and then incubated at 37 °C/5% CO_2 in 48-well cell culture plates containing PBS (pH = 7.4) solution (PBS solution changed daily). W_0 represents the initial weight of the hydrogels. At predetermined time points the hydrogel samples were removed from the incubation and their weights after lyophilization were recorded as W_t. The degradation of the hydrogel was evaluated by comparing the initial weight (W_0) and the weight measured at certain time points

$$\text{weight loss}\ (\%) = [(W_0 - W_t)/W_0] \times 100\% \quad (3)$$

Protein Release Experiment. Bovine serum albumin (BSA) with a comparable molecular weight to Mydgf was used as a model protein to conduct the release experiment. BSA was added to PPC-ET precursor solution and then mixed with PEG solution to form protein-loaded hydrogels in situ as described above. The yielded BSA-loaded hydrogel disk samples were incubated in 2 mL of PBS (changed daily) at 37 °C (n = 5 per group). A 200 μL aliquot of the incubation media for each sample was analyzed at defined time points using high-performance liquid chromatography (HPLC).

Cytotoxicity and Cell Adhesion Studies. Before the studies, precursor solutions and hydrogels were sterilized by 70% ethanol and UV light. Each sample was immersed in 1 mL Dulbecco's modified Eagle's medium (DMEM) at 37 °C/5% CO_2 for 72 h. The extract of hydrogel was added with 10% fetal bovine serum (FBS). The NIH-3T3 cells were seeded at a density of 5×10^4 in cell culture plates (96-well) and incubated at 37 °C/5% CO_2 in high-glucose DMEM containing 10% FBS, 100 μg/mL streptomycin, and 100 units/mL penicillin for 24 h. Next, the cell culture medium was removed from the cell culture plates and replaced with the hydrogel extract. XTT assay was performed according to the manufacturer's instructions after an additional 48 h culture, and cell culture plates were used as control.

CRGDS-modified hydrogel (PPC-ET/CRGDS-PEG) disk samples with a CRGDS concentration of 0.1 wt % were casted in 96-well cell culture plates (Fisher Scientific, Pittsburgh, PA) to determine if the hydrogel biomaterials supported cell adhesion and proliferation. The PPC-ET/CRGDS-PEG hydrogel samples were sterilized by 70% ethanol and UV light prior to use. Ten thousand cells/cm^2 of NIH-3T3 cells were seeded onto each hydrogel sample and allowed to incubate at 37 °C/5% CO_2 to facilitate cell attachment (cell culture media changed daily). Microscopy (Keyence, Itasca, IL) was used as the observation instrument of cell morphology.

Effects of Mydgf Composite Hydrogels on the Vascularization of HUVECs. HUVECs were used for this in vitro tube-formation assay. The growth factor-reduced basement membrane extract Matrigel was used as a culture substratum. Hydrogel solutions were sterilized by filtration before use, and a thin layer of PPC-ET/PEG hydrogels (300 μL) and Mydgf-loaded hydrogels (50 ng/mL) were laid over the prechilled 96-well culture plates, while the control group was coated with growth factor-reduced Matrigel matrix until completely solidified. HUVECs were cultured in Dulbecco's Modified Eagle Medium/F12 (DMEM/F12; Invitrogen). Trypsinized HUVECs resuspended in DMEM medium with only PBS and Mydgf (50 ng/mL) were added to the preconditioned culture plates at a density of 2×10^4 cells/well. After incubation at 37 °C with 5% CO_2 for 8 h, nonadherent HUVECs in the culture plates were washed with PBS. HUVEC cells were imaged, and the tubular numbers were counted to evaluate the tube formation ability. Image-Pro Plus software (Media Cybernetics Inc., Bethesda, MD, USA) was used to evaluate the tubular length and tubular intersecting nodes in five random fields (200×) based on Mirshahi's method.[28] Each experiment was performed three times.

Experimental MI Model and Hydrogel Injection. Male Sprague–Dawley (SD) rats (220–250 g, 6–8 weeks) used in this study were purchased from the Laboratory Animal Care Facility (LACF) of the Shanghai Jiao Tong University School of Medicine. The procedures involving animals adhered to the principles of the Guide for the Care and Use of Laboratory Animals of the Institute for Laboratory Animal Research. Rats were anesthetized with sodium pentobarbital (30 mg/kg, i.p.), orally tracheal intubated, and ventilated with air at a respiratory rate of 80 times/min. After a left thoracotomy was finished in the fourth ribs intercostal, the LAD (about 2 mm below the level of the left atrial appendage) was exposed and ligated permanently with 6–0 polypropylene (Ethicon, Somerville, USA) for induction of acute myocardial infarction (AMI) model. Successful AMI was confirmed by LV ligation regional wall pale and ST-segment elevation on an electrocardiogram (ECG) device. Syringes with PBS (MI-only), control hydrogel (no Mydgf), Mydgf, and Mydgf–hydrogel (10 μg Mydgf was encapsulated in 120 μL sterile well-mixed hydrogel precursor solutions) were prepared during the surgery. Separate hydrogels were prepared for each rat to maintain

DOI: 10.1021/acsami.9b12043
ACS Appl. Mater. Interfaces 2019, 11, 38429–38439

sterility and avoid cross-contamination. After LAD ligation, the heart was to receive one of the above four treatments randomly: a 29-gauge insulin needle (BD Biosciences) was utilized to insert the injection into the peri-infarct LV wall and directed toward the MI zone. A total volume of 120 μL was injected directly into 3 locations after LAD ligation, and the needle was withdrawn slowly to avoid material leakage. The thorax was then closed, and the rat was placed on a warm plate.

Cardiac Echocardiography and microPET Measurements. Two days after experiencing MI, the baseline echocardiographic measurements were collected. Assessment of the LV cardiac function and structure was through operation of the Vevo 2100 ultrasound Imaging System (VisualSonics, Canada). The echocardiography was operated by an experienced and blinded technician. Collection and analysis of echocardiographic data proceeded 2 days after ligation (baseline) and 4 weeks after injection.[24] Rats received echocardiography 2 days after permanent LAD ligation (baseline) and 4 weeks post-treatment to measure cardiac function and structure indicators such as LVIDs, LVIDd, LVEF, and LVFS. All parameters were measured based on the mean of three consecutive cardiac cycles. These high-quality images were determined from short-axis 2-dimensional imaging at the midaxillary level.

Myocardial viability was measured with a dedicated small-animal PET system (MOSAIC; Philips). After being anesthetized, the rats were given an intravenous injection of ^{18}F-FDG (37 MBq) through the tail vein. The rats were subjected to intraperitoneal administration of glucose (1 mg/g body weight) and insulin (8 mUI/g body weight) to improve the myocardium uptake tracer in 30 min before the ^{18}F-FDG injection. The ^{18}F-FDG imaging acquisition started 30 min after ^{18}F-FDG administration and continued for 30 min. The small-animal micro-PET system was operated by an experienced and blinded technician. LV defect size was defined by the fraction of polar map elements with decreased tracer uptake in the total polar map derived from the ^{18}F-FDG uptake.[29]

Haematoxylin and Eosin, Masson Trichrome Staining. At 4 weeks following the injection, the rats (n = 8 in each group) were euthanized and the heart tissue was collected. The hearts were rinsed with 4% formaldehyde for 20 min and then rinsed with PBS for about 10 min. Then the hearts were divided into 5 pieces in the transverse orientation to the apex at 2 mm intervals. Heart samples were fixed, embedded in paraffin, and then sectioned into 5 μm slices for subsequent histopathological and morphometric analyses. Masson's trichrome-stained slides were performed from the closest section plane.

The following data was measured using ImageJ software: the ventricular wall thickness, scar thickness (mm), septum thickness (mm), LV cavity area (mm^2), and whole LV area (mm^2). Each measurement was performed three times. Relative scar thickness was calculated as the ratio of the average thickness of the scar wall to the average thickness of the uninfarcted wall. The infarct expansion index was calculated as follows: (LV cavity area/whole LV area)/relative scar thickness.[30]

Immunocytochemistry Staining. Immunofluorescence was carried out to identify blood vessel formation. Blood vessels were stained with a primary antibody against CD31 (AF3628-SP, R&D) and an antibody against alpha smooth muscle actin (α-SMA) (A2547, Sigma). An LSM710 Meta confocal microscope (Carl Zeiss, Feldbach, Switzerland) was utilized for confocal images. The quantification of the arterioles and capillaries was calculated separately. The capillary density values are calculated as the mean within 1 mm^2 areas in 5 random fields, and the maturation index was calculated on the basis of the number of α-SMA-positive vessels relative to the total number of vessels.

Terminal Deoxynucleotidyl Transferase dUTP Nick-End Labeling (TUNEL) Staining. TUNEL staining of tissue cross sections from LV papillary muscle regions of all groups was performed. For each slide, 5 separate fields were randomly selected. Cells with clear nuclear labeling were defined as TUNEL-positive cells. The numbers of TUNEL-positive nuclei or total nuclei were calculated with ImageJ. The apoptotic index was defined as the ratio of the number of TUNEL-positive nuclei versus the total number of nuclei.

Statistical Analysis. GraphPad Prism 6.0 software (La Jolla, CA) and SPSS19 (IBM) statistics software were utilized for statistical analysis. Unpaired two-tailed student's test was applied to compare the difference between two groups; the one-way ANOVA analysis with Tukey posthoc test was also used to identify the difference between groups. Data were presented as mean ± standard deviation. A value of $p < 0.05$ was considered to denote statistical significance.

■ ASSOCIATED CONTENT

Supporting Information

The Supporting Information is available free of charge on the ACS Publications website at DOI: 10.1021/acsami.9b12043.

Characterization of PPC/PPC-ET oligomers; fabrication of PPC-ET/8arm PEG-Maleimide; angiogenic effect of citrate for upregulating the expression of CD31 and VEGF in HUVECs; echocardiographic evaluation of cardiac function 2 days after ligation; effects of the Mydgf–hydrogel on cell apoptosis (PDF)

■ AUTHOR INFORMATION

Corresponding Authors

*E-mail: zq11607@rjh.com.cn.
*E-mail: xiaofengye@hotmail.com.
*E-mail: xiaoyang@njit.edu.

ORCID

Xiaofeng Ye: 0000-0001-9307-636X
Xiaoyang Xu: 0000-0002-1634-3329

Author Contributions

‖Z.Y., Y.-H.T., and X.-Q.Z. contributed equally to this work.

Notes

The authors declare no competing financial interest.

■ ACKNOWLEDGMENTS

This work was supported by American Heart Association grant no. 19AIREA34380849 (X.X.). X.X. acknowledges support from the New Jersey Institute of Technology (NJIT) startup funding, the New Jersey Health Foundation (PC102-17 and PC25-18), and the NSF Innovation Corps program (1723667). Q.Z. and X.F.Y. acknowledge support from the National Natural Science Foundation of China (Grants 81671832 and 81571826). X.-Q.Z. acknowledges support from the Interdisciplinary Program of Shanghai Jiao Tong University (project number ZH2018ZDA36 (19X190020006)).

■ REFERENCES

(1) Seliktar, D. Designing Cell-Compatible Hydrogels for Biomedical Applications. *Science* **2012**, *336* (6085), 1124–1128.
(2) Nguyen, M. K.; Lee, D. S. Injectable Biodegradable Hydrogels. *Macromol. Biosci.* **2010**, *10* (6), 563–579.
(3) Ma, C. Y.; Gerhard, E.; Lu, D.; Yang, J. Citrate chemistry and biology for biomaterials design. *Biomaterials* **2018**, *178*, 383–400.
(4) Lampe, K. J.; Namba, R. M.; Silverman, T. R.; Bjugstad, K. B.; Mahoney, M. J. Impact of Lactic Acid on Cell Proliferation and Free Radical-Induced Cell Death in Monolayer Cultures of Neural Precursor Cells. *Biotechnol. Bioeng.* **2009**, *103* (6), 1214–1223.
(5) Lv, H. W.; Wang, H. P.; Zhang, Z. J.; Yang, W.; Liu, W. B.; Li, Y. L.; Li, L. S. Biomaterial stiffness determines stem cell fate. *Life Sci.* **2017**, *178*, 42–48.

DOI: 10.1021/acsami.9b12043
ACS Appl. Mater. Interfaces 2019, 11, 38429–38439

(6) Tsou, Y.-H.; Khoneisser, J.; Huang, P.-C.; Xu, X. Hydrogel as a bioactive material to regulate stem cell fate. *Bioact. Mater.* **2016**, *1* (1), 39−55.
(7) Yildirimer, L.; Seifalian, A. M. Three-dimensional biomaterial degradation - Material choice, design and extrinsic factor considerations. *Biotechnol. Adv.* **2014**, *32* (5), 984−999.
(8) Zhang, H.; Zhou, L.; Zhang, W. Control of Scaffold Degradation in Tissue Engineering: A Review. *Tissue Eng., Part B* **2014**, *20* (5), 492−502.
(9) Ma, C. Y.; Tian, X. G.; Kim, J. P.; Xie, D. H.; Ao, X.; Shan, D. Y.; Lin, Q. L.; Hudock, M. R.; Bai, X. C.; Yang, J. Citrate-based materials fuel human stem cells by metabonegenic regulation. *Proc. Natl. Acad. Sci. U. S. A.* **2018**, *115* (50), E11741−E11750.
(10) Xie, D. H.; Guo, J. S.; Mehdizadeh, M. R.; Tran, R. T.; Chen, R. S.; Sun, D. W.; Qian, G. Y.; Jin, D. D.; Bai, X. C.; Yang, J. Development of injectable citrate-based bioadhesive bone implants. *J. Mater. Chem. B* **2015**, *3* (3), 387−398.
(11) Binu, S.; Soumya, S. J.; Sudhakaran, P. R. Metabolite control of angiogenesis: angiogenic effect of citrate. *J. Physiol. Biochem.* **2013**, *69* (3), 383−395.
(12) Tran, R. T.; Wang, L.; Zhang, C.; Huang, M. J.; Tang, W. J.; Zhang, C.; Zhang, Z. M.; Jin, D. D.; Banik, B.; Brown, J. L.; Xie, Z. W.; Bai, X. C.; Yang, J. Synthesis and characterization of biomimetic citrate-based biodegradable composites. *J. Biomed. Mater. Res., Part A* **2014**, *102* (8), 2521−2532.
(13) Martinez-Outschoorn, U. E.; Peiris-Pages, M.; Pestell, R. G.; Sotgia, F.; Lisanti, M. P. Cancer metabolism: a therapeutic perspective. *Nat. Rev. Clin. Oncol.* **2017**, *14* (1), 11−31.
(14) Mills, E. L.; Kelly, B.; O'Neill, L. A. J. Mitochondria are the powerhouses of immunity. *Nat. Immunol.* **2017**, *18* (5), 488−498.
(15) Benjamin, E. J.; Blaha, M. J.; Chiuve, S. E.; Cushman, M.; Das, S. R.; Deo, R.; Floyd, J.; Fornage, M.; Gillespie, C.; Isasi, C. Heart disease and stroke statistics-2017 update: a report from the American Heart Association. *Circulation* **2017**, *135* (10), e146−e603.
(16) Hasan, A.; Khattab, A.; Islam, M. A.; Hweij, K. A.; Zeitouny, J.; Waters, R.; Sayegh, M.; Hossain, M. M.; Paul, A. Injectable Hydrogels for Cardiac Tissue Repair after Myocardial Infarction. *AdvSci. (Weinh)* **2015**, *2* (11), 1500122.
(17) Korf-Klingebiel, M.; Reboll, M. R.; Klede, S.; Brod, T.; Pich, A.; Polten, F.; Napp, L. C.; Bauersachs, J.; Ganser, A.; Brinkmann, E. Myeloid-derived growth factor (C19orf10) mediates cardiac repair following myocardial infarction. *Nat. Med.* **2015**, *21* (2), 140.
(18) Cully, M. Cardiovascular disease: MYDGF promotes heart repair after myocardial infarction. *Nat. Rev. Drug Discovery* **2015**, *14* (3), 164.
(19) Pritchard, C. D.; O'Shea, T. M.; Siegwart, D. J.; Calo, E.; Anderson, D. G.; Reynolds, F. M.; Thomas, J. A.; Slotkin, J. R.; Woodard, E. J.; Langer, R. An injectable thiol-acrylate poly (ethylene glycol) hydrogel for sustained release of methylprednisolone sodium succinate. *Biomaterials* **2011**, *32* (2), 587−597.
(20) Zhou, Y.; Nie, W.; Zhao, J.; Yuan, X. Rapidly in situ forming adhesive hydrogel based on a PEG-maleimide modified polypeptide through Michael addition. *J. Mater. Sci.: Mater. Med.* **2013**, *24* (10), 2277−2286.
(21) Westman, P. C.; Lipinski, M. J.; Luger, D.; Waksman, R.; Bonow, R. O.; Wu, E.; Epstein, S. E. Inflammation as a driver of adverse left ventricular remodeling after acute myocardial infarction. *J. Am. Coll. Cardiol.* **2016**, *67* (17), 2050−2060.
(22) Michelis, K. C.; Boehm, M.; Kovacic, J. C. New vessel formation in the context of cardiomyocyte regeneration−the role and importance of an adequate perfusing vasculature. *Stem Cell Res.* **2014**, *13* (3), 666−682.
(23) Prabhu, S. D.; Frangogiannis, N. G. The biological basis for cardiac repair after myocardial infarction: from inflammation to fibrosis. *Circ. Res.* **2016**, *119* (1), 91−112.
(24) Paul, A.; Hasan, A.; Kindi, H. A.; Gaharwar, A. K.; Rao, V. T.; Nikkhah, M.; Shin, S. R.; Krafft, D.; Dokmeci, M. R.; Shum-Tim, D. Injectable graphene oxide/hydrogel-based angiogenic gene delivery system for vasculogenesis and cardiac repair. *ACS Nano* **2014**, *8* (8), 8050−8062.
(25) Takwa, M.; Simpson, N.; Malmström, E.; Hult, K.; Martinelle, M. One-Pot Difunctionalization of Poly (ω-pentadecalactone) with Thiol-Thiol or Thiol-Acrylate Groups, Catalyzed by Candida antarctica Lipase B. *Macromol. Rapid Commun.* **2006**, *27* (22), 1932−1936.
(26) Phelps, E. A.; Enemchukwu, N. O.; Fiore, V. F.; Sy, J. C.; Murthy, N.; Sulchek, T. A.; Barker, T. H.; García, A. J. Maleimide cross-linked bioactive peg hydrogel exhibits improved reaction kinetics and cross-linking for cell encapsulation and in situ delivery. *Adv. Mater.* **2012**, *24* (1), 64−70.
(27) Zhang, Y.; Liu, J.; Huang, L.; Wang, Z.; Wang, L. Design and performance of a sericin-alginate interpenetrating network hydrogel for cell and drug delivery. *Sci. Rep* **2015**, *5*, 123741.
(28) Mirshahi, P.; Rafii, A.; Vincent, L.; Berthaut, A.; Varin, R.; Kalantar, G.; Marzac, C.; Calandini, O.; Marie, J.; Soria, C. Vasculogenic mimicry of acute leukemic bone marrow stromal cells. *Leukemia* **2009**, *23* (6), 1039.
(29) Kudo, T.; Fukuchi, K.; Annala, A. J.; Chatziioannou, A. F.; Allada, V.; Dahlbom, M.; Tai, Y.-C.; Inubushi, M.; Huang, S.-C.; Cherry, S. R. Noninvasive measurement of myocardial activity concentrations and perfusion defect sizes in rats with a new small-animal positron emission tomograph. *Circulation* **2002**, *106* (1), 118−123.
(30) Alhaddad, I. A.; Tkaczevski, L.; Siddiqui, F.; Mir, R.; Brown, E. J. Aspirin enhances the benefits of late reperfusion on infarct shape: A possible mechanism of the beneficial effects of aspirin on survival after acute myocardial infarction. *Circulation* **1995**, *91* (11), 2819−2823.

DOI: 10.1021/acsami.9b12043
ACS Appl. Mater. Interfaces 2019, 11, 38429−38439